Proceedings, Bicycle and Motorcycle Dynamics 2010
Symposium on the Dynamics and Control of Single Track Vehicles,
20 - 22 October 2010, Delft, The Netherlands

Comparison of a Bicycle Steady-State Turning Model to Experimental Data

S. M. Cain[*] and N. C. Perkins[#]

[*]Department of Biomedical Engineering
University of Michigan
2200 Bonisteel Blvd., Ann Arbor, MI, 48109 USA
e-mail: smcain@umich.edu

[#]Department of Mechanical Engineering
University of Michigan
2350 Hayward St., Ann Arbor, MI, 48109 USA
e-mail: ncp@umich.edu

ABSTRACT

We investigate the steady-state handling of a bicycle as the means to explore the major factors governing the maneuverability and handling characteristics of a rider/bicycle system. Steady-state handling arises when the rider/bicycle negotiates a constant radius turn at constant speed and lean. Employing a bicycle instrumented to measure steering torque, steering angle, bicycle speed, bicycle acceleration, and bicycle angular velocity, we report data for 108 trials. The trials include two subjects executing steady turns of six different radii, at three speeds, and with three rider lean conditions. We introduce a model for the steady-state handling of the bicycle/rider system that accounts for rider lean and compare the experimental data to the model predictions. We find that the model, with idealized tire parameters, explains 97.0% of the variability in the measured bicycle roll angle, 99.6% of the variability in the measured steering angle, and 88.8% of the variability in the measured steering torque. Using more realistic tire parameters yields little difference in the model predictions. Both the model and the data demonstrate that rider lean (lateral shifting of the bicycle/rider center of mass) strongly influences the steering torque/lateral acceleration ratio, suggesting that rider lean plays an important role in the control of a bicycle. By contrast, the steering angle/lateral acceleration ratio is largely insensitive to rider lean, suggesting that using the steering angle as a cue for bicycle control is advantageous over using steering torque.

Keywords: instrumented bicycle, steady turning, rider lean, steering torque.

1 INTRODUCTION

The design of the modern bicycle is the result of almost two centuries of trial and error. Recent research has helped us to understand the stability of a bicycle [1] and has shown that the current bicycle configuration could be made more stable with relatively small adjustments to standard bicycle geometry [2]. However, stability is not the only characteristic that a human rider desires; a bicycle also needs to be maneuverable and have desirable handling characteristics.

A first step towards understanding the maneuverability of a bicycle is to examine its handling characteristics during steady-state turning. The theoretical steady-state turning behavior of bicycles has been investigated most recently by Basu-Mandal et al. [3] and Peterson and Hubbard [4]. Basu-Mandal et al. employed the nonlinear equations of motion for an idealized benchmark bicycle to identify hands-free, (zero applied steer torque) steady-state turning motions. In so doing, they provide evidence that a human rider is not required to impart large steering torques during steady-state turning. Peterson and Hubbard used the benchmark bicycle model to identify all kinematically feasible steady-turns and relate the steering torque and velocity needed to develop each turn. Their model reveals that the sign of the steering torque can change depending on the configuration of the bicycle, which has important implications for bicycle control.

Related to the steady-state behavior of bicycles are numerous theoretical and experimental studies of the steady-state turning of motorcycles. Fu [5] developed a model for steady-state turning, and tested this model using a motorcycle equipped with steering angle and lean angle sensors. Experimental measurements of the motorcycle lean angle matched those predicted by the model and confirmed the importance of gyroscopic effects. The measured steering angles were somewhat less than theoretical predictions, suggesting that the lateral tire force develops mainly from tire camber as opposed to tire side slip. Cossalter et al. [6] developed a mathematical model of the steering torque as a function of speed, turn radius, tire properties, and motorcycle geometry/mass distribution. Doing so revealed the acceleration index , the ratio of the steering torque and lateral acceleration, as a fundamental measure of motorcycle maneuverability [6-8]. Bortoluzzi et al. [7] constructed an instrumented motorcycle capable of measuring steering torque, steering angle, roll angle, velocity, roll rate, and yaw rate for the purpose of testing a steady-state model similar to that of Cossalter et al. The measured acceleration index remained in good agreement with theoretical predictions and was relatively insensitive to changes in tire properties and rider mass distribution. By contrast, the lateral displacement (i.e., the lean) of the rider had a pronounced effect on the acceleration index, especially at smaller lateral accelerations.

While bicycles and motorcycles share common features as two-wheeled single-track vehicles, there are also key distinctions. For a bicycle, a rider may comprise 85-95% of the total mass, whereas for a motorcycle, a rider may only account for 15-30% of the total mass [9]. When the ratio of vehicle to rider mass is large (i.e., for motorcycles), the rider steering torque is the dominant control input [6]. By contrast, when the vehicle/rider mass ratio is small (i.e., for bicycles), other control mechanisms arise, such as upper body lean and knee movement [10].

Instrumented bicycles have been used to investigate the human control and dynamic behavior of bicycles. Roland [11] instrumented a bicycle to measure steering angle, bicycle roll angle, forward velocity of the bicycle, and rider lean angle in order to verify simulation results of a riderless bicycle and to analyze the steer and lean control used by a human rider. Jackson and Dragovan [12] instrumented a bicycle to measure bicycle speed, angular velocity of the bicycle, and steering angle. They used measurements collected during no-hands riding in conjunction with simplified equations of motion to investigate the contributions of the torque applied to the front wheel by the ground reaction force and the gyroscopic moment. They report reasonable agreement with theory. Cheng et al. [13] instrumented a bicycle to measure steering torque during turning maneuvers. They found that larger steering torques are required to initiate turns developed by larger steering angles as expected. Kooijman et al. [14] instrumented a riderless bicycle with angular rate sensors, a steering angle sensor, and a forward speed sensor to validate a model of an uncontrolled bicycle, and found the model to be reasonably accurate for the low-speed behavior. Most recently, Kooijman and Schwab [15] instrumented a bicycle to record lean, yaw and steering rates, steering angle, rear wheel speed, and pedaling cadence frequency. Their bicycle was also equipped with a video camera to record rider motion. They found that during normal cycling on a treadmill and on a short outdoor circuit, most control was done through steering as opposed to upper body lean.

The objective of this paper is to develop a theoretical model to explore the major factors governing the maneuverability and handling characteristics of the rider/bicycle system and to evaluate model fidelity via an instrumented bicycle. To this end, we focus on steady-state handling as defined by a negotiating a constant radius turn at constant speed and lean. We open our Methods Section by introducing a novel instrumented bicycle that incorporates sensors to detect steering torque, steering angle, bicycle speed, and the acceleration and angular velocity of the bicycle. We then introduce a model for the steady-state handling of the bicycle/rider system that also accounts for rider lean. The Results and Discussion Sections summarize substantial comparisons of experimental and theoretical results for the bicycle roll angle, steering angle, and steering torque. We observe that rider lean (lateral shifting of the bicycle/rider center of mass) strongly influences the steering torque/lateral acceleration ratio, suggesting that rider lean plays an important role in the control of a bicycle. By contrast, the steering angle/lateral acceleration ratio is largely insensitive to rider lean, suggesting that using the steering angle as a cue for bicycle control is advantageous over using steering torque. These findings have important implications for understanding human control of a bicycle.

2 METHODS

2.1 Instrumented bicycle

An instrumented bicycle was constructed to measure the major variables that define the steady state handling of a bicycle. In the following, we describe the bicycle, the sensors, the power supplies and the data acquisition system.

2.1.1 Bicycle

The bicycle shown in Figure 1 is a standard geometry (head angle = 72 degrees, trail = 58 mm, wheelbase = 1.047 m), rigid (unsuspended) mountain bike equipped with 660.4 mm x 49.5 mm (26 in x 1.95 in) slick tires. The wheel bearings were properly adjusted and the wheels were trued by a professional bicycle mechanic prior to testing.

Figure 1. The instrumented bicycle. The instrumented bicycle is a standard geometry mountain bike equipped to measure: steering torque, steering angle, bicycle speed, bicycle angular velocity about three axes, and acceleration along three axes. A laptop computer, A/D boards, battery, and circuitry are supported in a box at the rear.

2.1.2 Instrumentation

The instrumentation selected for this study enabled the simultaneous measurement of the steering torque, the steering angle, the bicycle speed, and the acceleration and angular velocity of the bicycle frame.

Steering torque. We constructed the custom instrumented fork shown in Figure 2 to measure the steering torque. The placement of a torque sensor (Transducer Techniques SWS-20) within the steerer tube permitted the measurement of the torque transmitted between the handlebars and the front wheel. We isolated the torque sensor from unwanted bending moments and axial loading by using an angular contact bearing (Enduro 7901). Following installation, we calibrated the torque sensor *in situ* by orienting the bicycle such that the steering axis was parallel to the ground, securing a long length of threaded rod in the fork dropouts, and then placing known masses at measured distances from the steering axis to create known torques. Following calibration, we measured the stiffness of the torque sensor to be 4.97 Nm/deg. The signal from the torque sensor was amplified using a load cell signal conditioner (Transducer Techniques TMO-1) and was sampled at 1000Hz in the experiments described below.

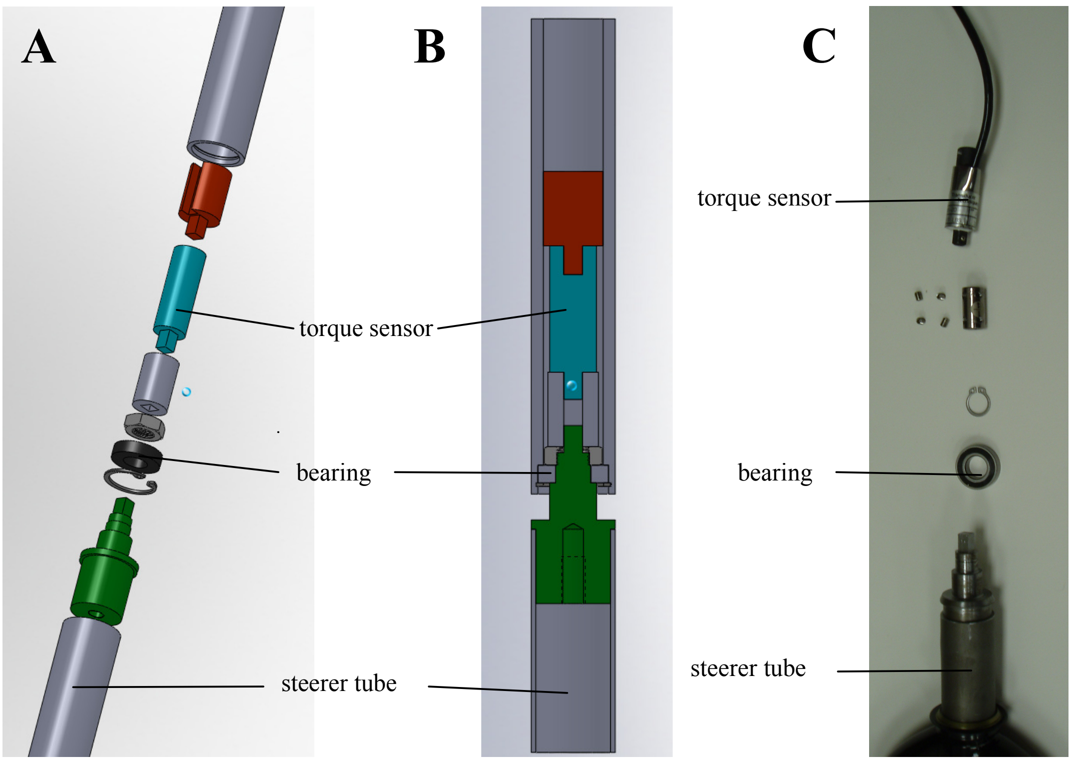

Figure 2. The instrumented fork. We constructed a custom instrumented fork to measure steering torque. **(A)** An exploded view of the steerer tube of the instrumented fork. **(B)** A section view of the assembled instrumented fork. **(C)** A photograph of the disassembled instrumented fork.

Steering angle. We employed an optical encoder to measure the steering angle. We secured a custom encoder disk (US Digital HUBDISK-2-1800-1125-I) to the bicycle fork similar to a headset spacer as illustrated in Figure 3. We attached the encoder module (US Digital EM1-2-1800) to a custom aluminum plate, which was secured to the bicycle frame by using the top headset race as shown in Figure 3. An encoder chip (US Digital LFLS7183) was used to convert the raw signal from the encoder module to up and down counts and was sampled at 200 Hz. The optical encoder measured the steering angle with a resolution of 0.1 degrees.

Figure 3. The encoder and encoder disk used to measure the steering angle. The encoder module was fastened to a custom aluminum plate secured to the bicycle frame using the upper headset cup. The encoder disk was secured to the steering tube of the fork, similar to a headset spacer.

Bicycle speed. We calculated bicycle speed by measuring revolutions of the front wheel and then multiplying the number of revolutions per unit time by the circumference of the front wheel. Wheel revolutions were measured using a magnetic reed switch (Cateye 169-9772) and a single wheel mounted magnet (Cateye 169-9691). We sampled the signal from the magnetic reed switch at 1000 Hz.

Acceleration and angular velocity. A custom inertial measurement unit (IMU) shown in Figure 4 was constructed using a three-axis accelerometer (Analog Devices ADXL335) and three single-axis angular rate gyros (Murata ENC-03M). We secured the IMU to a custom aluminum plate which is fastened to the seat tube of the bicycle frame utilizing the water bottle cage mounting holes (Figure 4). The angular velocity measurements were used to calculate the turn radius and the acceleration measurements were used to calculate the bicycle roll angle as further described in Section 2.3. The signals from the accelerometer and three angular rate gyros were sampled at 1000 Hz. The IMU was calibrated using the technique described by King [16].

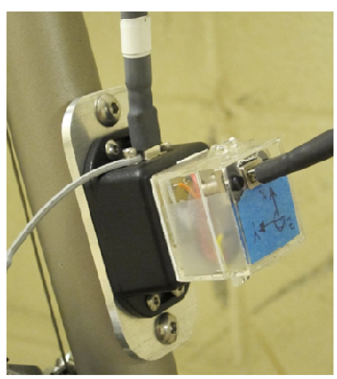

Figure 4. A custom inertial measurement unit (IMU). The IMU was secured to a custom aluminum plate which was fastened to the bicycle by utilizing the water bottle cage mounting holes.

Data acquisition. We used a small laptop computer (Dell Inspiron mini) running a custom LabVIEW (National Instruments) program and two data acquisition boards (National Instruments USB-6008) to convert analog signals to digital and to log data collected during each trial. The laptop and data acquisition boards were carried in a foam-padded wooden box mounted to the rear of the bicycle (Figure 1).

Power Supplies. Four 3.7 volt, 900 mAh polymer lithium ion batteries (Sparkfun PRT-00341) were used to supply power to the instrumentation. We created the required voltage for each sensor by wiring the required number of batteries in series. Voltage for each sensor was regulated by a step-up / step-down switching DC-DC converter (All-Battery.com, AnyVolt Micro).

2. 2 Experimental protocol

Two subjects rode the instrumented bicycle around a course containing six curves of constant radius (radii 9.14, 12.19, 18.29, 22.86, 27.43, and 30.48 meters). All of the curves, located outdoors on smooth and level pavement, were clearly marked with chalk. Each subject selected his or her seat height and remained seated during each trial. We instructed the subjects to ride the course three times and at constant speeds that the subjects considered to be slow, medium, and fast. A bicycle computer with a visual display (Cateye Velo 8) allowed subjects to monitor their speed if desired. It is important to note that subjects were required to pedal the bicycle to maintain speed; no motors were used to remove the task of pedaling. Allowing the subjects to select approximate slow, medium, and fast speeds eliminated the additional mental task associated with requiring them to maintain a prescribed speed. As a result, each subject chose speeds corresponding to his or her preferred pedaling frequency (cadence). Furthermore, for a given curve and speed, the subjects were instructed to complete three trials distinguished by the degree of rider lean: natural rider lean, exaggerated rider lean into the turn, and exaggerated rider lean out of the turn. In summary, 54 trials were recorded for each subject: 6 curves x 3 speeds x 3 rider lean conditions. Prior to these trials, the tire pressure was set to 276 kPa (40 psi). In addition, we experimentally measured the normal force on each wheel by placing a scale under the wheel of interest while the subject sat on the bicycle in his/her preferred riding posture.

2.3 Data analysis

We first reviewed the data for each trial to identify time periods of steady-state turning as seen in the example of Figure 5. During steady-state turning, the bicycle speed, roll rate, steering angle, and turn radius remain nearly constant. Through visual inspection of bicycle speed, roll rate, steering angle, and turn radius, we selected areas of potential steady-state turning from each trial. We then analyzed each period of steady-turning by parsing this data into five-second blocks that were also shifted by 0.5 seconds. As a result, the first block of data began at the beginning of the period of steady turning, the second block of data began 0.5 seconds after the beginning of the period, and so on. The data for each five-second block was then averaged (to filter any modest transients) and this averaged data was used for all subsequent calculations described in the following. We used the following criteria to determine whether or not a block of data was considered steady-state:

- The magnitude of the forward acceleration of the bicycle during a five-second block, as calculated from the bicycle speed, must be less than or equal to 0.1 m/s^2.
- The standard deviation of the steering angle for a five-second block must not exceed three degrees.

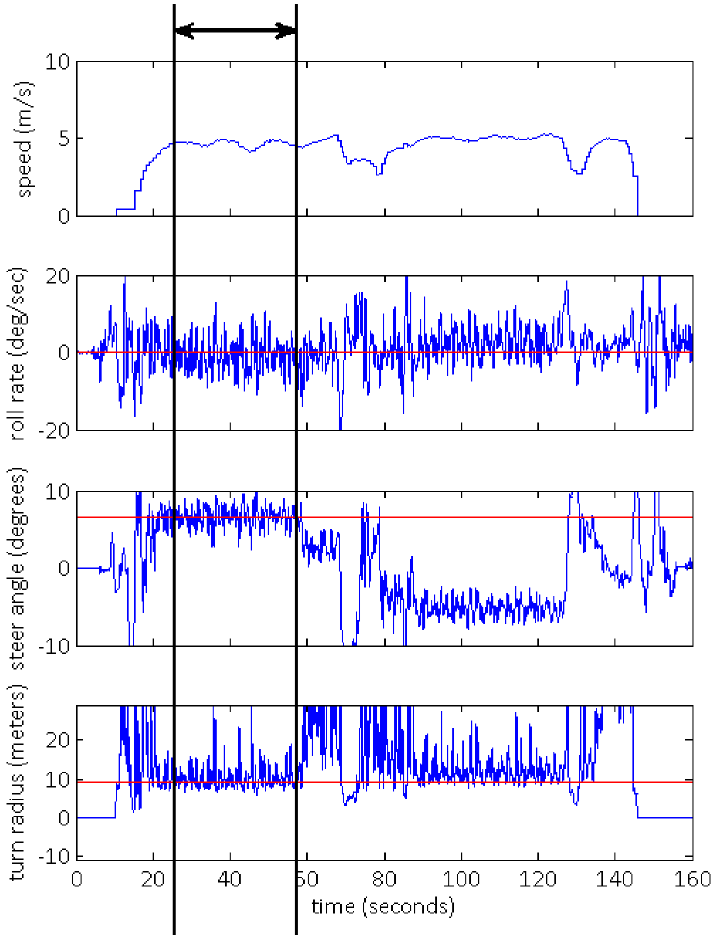

Figure 5. Identification of a region of steady-state turning. Bicycle speed, roll rate, steering angle, and instantaneous turn radius were used to identify a region of steady-state turning for processing. The region of steady turning for the example trial shown (a medium speed, clockwise turn with a turn radius of 9.14 meters) lies within the two vertical (black) lines. Another large region of steady-state turning begins around 90 seconds and ends at approximately 125 seconds. The turn radius data has been truncated to highlight the steady-state turning region of interest.

The inertial measurement unit defines a sensor frame of reference which differs from the bicycle-fixed frame illustrated in Figure 6A. The acceleration and angular velocity components measured in the sensor-fixed frame ($\overrightarrow{a_{123}}$ and $\overrightarrow{\omega_{123}}$) must be transformed into components measured in the bicycle-fixed frame ($\overrightarrow{a_{xyz}}$ and $\overrightarrow{\omega_{xyz}}$) for subsequent data reduction. This is achieved using, for example,

$$\overrightarrow{a_{xyz}} = \begin{bmatrix} cos\lambda & 0 & -sin\lambda \\ 0 & 1 & 0 \\ sin\lambda & 0 & cos\lambda \end{bmatrix} \overrightarrow{a_{123}} \tag{1}$$

where λ denotes the seat tube angle relative to vertical. The average radius of the turn for each five-second block was then determined from

$$R = \frac{\sqrt{\left((\omega_x)^2 + (\omega_y)^2\right)}}{u} \tag{2}$$

where u denotes the corresponding bicycle speed and ω_x and ω_y denote the angular velocities about the x and y axes illustrated in Figure 6B. The angular velocities ω_x and ω_y were determined using the outputs from the three sampled single-axis angular rate gyros. Note that upon assuming the pitch rate of the bicycle is negligible, the numerator of Equation (2) represents the yaw rate.

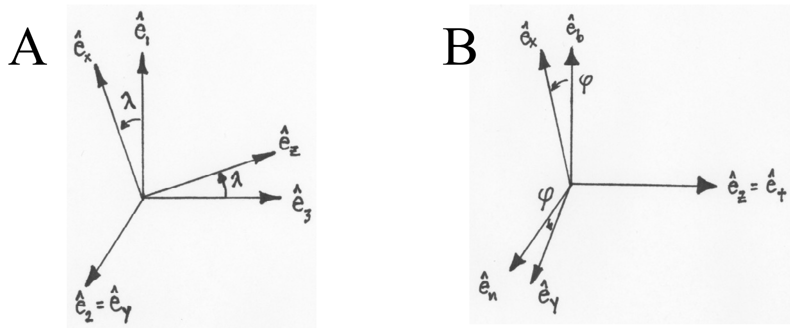

Figure 6. **(A)** The rotation of the bicycle-fixed frame $(\hat{e}_x, \hat{e}_y, \hat{e}_z)$ relative to the sensor-fixed frame $(\hat{e}_1, \hat{e}_2, \hat{e}_3)$. **(B)** The rotation of the bicycle-fixed frame relative to the inertial frame $(\hat{e}_b, \hat{e}_n, \hat{e}_t)$

The bicycle roll angle (φ) follows from the bicycle-fixed frame acceleration, $\overrightarrow{a_{xyz}}$, which includes the centripetal acceleration for steady turning (directed in the horizontal plane) and the acceleration due to gravity (directed along the vertical). For a clockwise turn, one of two equations is used to calculate roll angle, depending the direction of the measured acceleration along the bicycle fixed-frame y-axis (a_y).

For a clockwise turn with $a_y \leq 0$

$$\varphi = \left(\tan^{-1}\left(\frac{|a_y|}{|a_x|}\right) + \tan^{-1}\left(\frac{u^2}{Rg}\right)\right) \tag{3}$$

For a clockwise turn with $a_y > 0$

$$\varphi = \left(\tan^{-1}\left(\frac{u^2}{Rg}\right) - \tan^{-1}\left(\frac{|a_y|}{|a_x|}\right)\right) \tag{4}$$

where a_x and a_y are the values of the measured acceleration along the x and y axes defined in Figure 6.

Due to the placement of the steering angle optical encoder relative to the steering torque sensor, the angular displacement of the handlebar and stem about the steering axis ($\delta_{measured}$) was recorded instead of the angular displacement of the front wheel about the steering axis (δ_{true}). However, these values differ by a small but measurable twist of the assembly. The true steering angle, or angular displacement of the front wheel about the steering axis, is given by

$$\delta_{true} = \delta_{measured} - \frac{T_\delta}{4.97} \tag{5}$$

where T_δ is the measured steer torque and 4.97 Nm/deg is the aforementioned stiffness of the torque sensor assembly.

2.4 Theoretical model for steady-state handling

Our stated objective is to develop a fundamental understanding of the steady-state handling of a bicycle. To this end, and to complement the experimental procedure above, we developed a steady-state model for a bicycle making a turn of constant radius with constant speed and lean, similar to that for a vehicle [17, 18]. The model employs the following assumptions.

- Relative to the dominant forces (lateral tire forces and weight), air drag, longitudinal tire forces, and vertical tire moments are negligible.
- The turn radius (R) is much larger than the bicycle wheelbase (l).
- The steer angles remain small ($\delta < 10°$).
- The tires obey a linear elastic tire model.
- The pitch of the bicycle during turning remains negligible.
- The pneumatic trails of the tires remain negligible.
- The mechanical trail of the front wheel remains constant and independent of steer and lean.

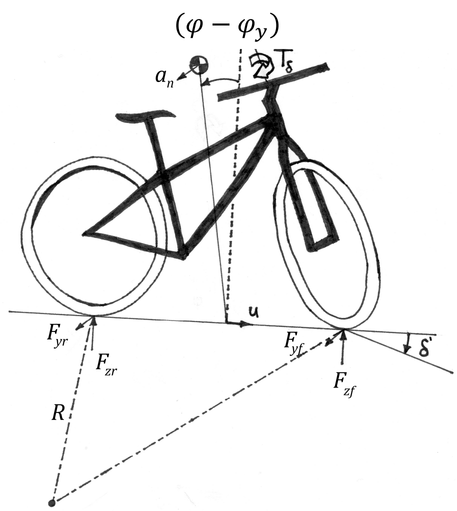

Figure 7. The bicycle in a steady-state turn. Important parameters are noted and are positive in the direction of the arrows.

The steady-state handling equations are derived from applying Newton's law in the lateral direction and moment equilibrium about the vertical axis. Figure 7 defines the bicycle model and the key variables. Solving Newton's law for the lateral tire forces yields

$$\frac{F_{yi}}{F_{zi}} = \frac{u^2}{Rg} = \frac{a_n}{g}, i = f, r \tag{6}$$

where i is an index used to denote the front ($i = f$) or rear ($i = r$) tire, F_y is the lateral tire force, F_z is the normal tire force, a_n is the lateral acceleration, and u and R are the forward speed and turn radius introduced above.

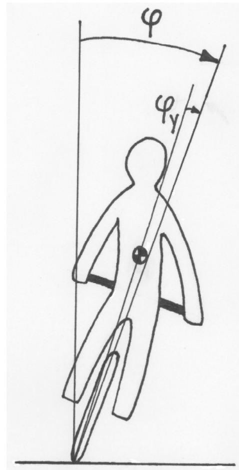

Figure 8. The additional roll angle of the bicycle caused by a leaning rider. For a clockwise turn, a rider can create a positive value of additional roll angle (φ_y) by leaning out of the turn. The arrows denote positive values for bicycle roll angle (φ) and the additional roll of the bicycle caused by rider lean (φ_y)

Recall that our experiments also allowed the rider to lean relative to the bicycle as seen in Figure 8. A leaning rider produces a lateral offset of the center of mass of the bicycle-rider system from the plane of the bicycle. The additional roll angle of the plane of the bicycle (φ_y) caused by this lateral offset is required for moment equilibrium about the longitudinal axis (aka the heading or x-axis). From this moment equilibrium equation, we deduce the following relationship between the roll angles and lateral acceleration:

$$a_n = g \tan(\varphi - \varphi_y) \tag{7}$$

where φ is the roll angle of the bicycle and φ_y is the additional roll angle caused by a rider leaning out of the plane of the bicycle. The camber of the (unsteered) rear tire is simply the roll angle of the bicycle

$$\gamma_r = \varphi \tag{8}$$

whereas the camber angle of the front tire

$$\gamma_f = \sin^{-1}(\sin\varphi + \delta\cos\varphi\sin\varepsilon) \tag{9}$$

also depends on the tilt of the steer axis ε and the steer angle δ where the small steer angle approximation is used again.

The linear elastic tire model accounting for tire side slip and camber [18] is given by

$$F_{yi} = C_{F\alpha i}\alpha_i + C_{F\gamma i}\gamma_i, i = f, r \tag{10}$$

where $C_{F\alpha}$ is the slip or cornering stiffness, α is the tire side slip angle, $C_{F\gamma}$ is the camber stiffness, and γ is the camber angle. In our study, we employ three sets of tire stiffness values: those from Roland [11] and Sharp [19] for elastic tires, and those for an idealized tire model [6] with infinite slip stiffness and zero camber stiffness ($C_{F\alpha} = \infty, C_{F\gamma} = 0$). The tire models of Roland and Sharp have been modified slightly for this study; namely, the nonlinear stiffness term (slip angle cubed) in the Roland model was neglected and the aligning stiffness term in the Sharp model was neglected. Table 1 provides a summary of the tire stiffness parameters used.

Table 1. Summary of the tire stiffness parameters used in this study.

Tire parameters	$C_{F\alpha}$ **(N/rad)**	$C_{F\gamma}$ **(N/rad)**
Idealized tire [6]	∞	0
Roland [11]	$F_{zi}[1 + (-4.88 \times 10^{-4} N^{-1})F_{zi}] \times 12.9$	$F_{zi}[1 + (-4.88 \times 10^{-4} N^{-1})F_{zi}] \times 0.186$
Sharp [19]	$14.325 \times F_{zi}$	$1 \times F_{zi}$

Solving Equations (6) – (10) for the slip angles for the front (α_f) and rear (α_r) tires yields

$$\alpha_f = \frac{1}{C_{F\alpha f}}\left(F_{zf} \tan\left(\varphi - \varphi_y\right) - C_{F\gamma f}\gamma_f\right) \tag{11}$$

$$\alpha_r = \frac{1}{C_{F\alpha r}}\left(F_{zr} \tan\left(\varphi - \varphi_y\right) - C_{F\gamma r}\gamma_r\right) \tag{12}$$

Under the assumptions of our model, the kinematics of a steady-turn [18] require that

$$R = \frac{l}{\delta' - \alpha_f + \alpha_r} \tag{13}$$

where δ' is the ground steer angle given by

$$\delta' = \frac{\delta \cos \varepsilon}{\cos \varphi - \delta \sin \varphi \sin \varepsilon} \tag{14}$$

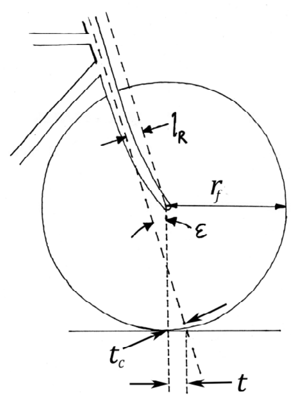

Figure 9. Front wheel assembly of a bicycle illustrating the dimensions and the geometric relationships between rake (l_R), front wheel radius (r_f), steer axis tilt (ε), trail (t), and mechanical trail (t_c). The mechanical trail is the perpendicular distance between the steering axis and the point of contact between the front wheel and the ground whereas the trail is the horizontal component of the mechanical trail.

Using the measured geometry from the instrumented bicycle, we calculate the trail (t) and the mechanical trail (t_c) illustrated in Figure 9 as

$$t = \frac{r_f \cos(\pi - \varepsilon) - l_R}{\sin(\pi - \varepsilon)} \tag{15}$$

$$t_c = t \cos(\varepsilon) \tag{16}$$

where r_f is the radius of the front wheel, ε again is the steer axis tilt (or π minus the head angle), and l_R is the fork rake. The steer torque (T_δ) required by the rider can then be found by summing the moments about the steering axis caused by the normal force (F_{zf}) and the lateral force (F_{yf}) acting on the front tire.

$$T_\delta = t_c F_{yf} \cos\gamma_f - t_c F_{zf} \sin\gamma_f \tag{17}$$

Solutions to the steady-state handling model above are found as follows. We begin by specifying the bicycle roll angle (φ), additional roll angle caused by rider lean (φ_y), and the steering angle (δ). These values are first used in Equations (7) – (9) to solve for the lateral acceleration and the camber angles of the front and rear tires. Next, the camber angles and roll angles are used in Equations (11) and (12) to solve for the slip angles of the front and rear tires. We then calculate the lateral tire force using Equation (10) and turn radius using Equation (13). Finally, we calculate the steering torque from Equation (17).

2.5 Comparison of the model to experimental data

In order to compare the model predictions to the experimental data, we used the measured bicycle speed (u), nominal turn radius (R), and bicycle roll angle (φ) as follows.

1. The lateral acceleration was calculated using Equation (6).
2. Using the measured bicycle roll angle, we calculated the additional roll of the bicycle caused by rider lean (φ_y) using Equation (7).
3. We solved for the predicted slip and camber angles of the rear tire using Equations (8) and (12).
4. We solved for the model predicted slip and camber angles of the front tire, steer angle, and ground steer angle by numerically solving Equations (9), (11), (13), and (14).
5. We calculated the predicted lateral tire force on the front tire using Equation (10).
6. Finally, we calculated the predicted steering torque using Equation (17).

We assumed that the weight distribution of the bicycle/rider system did not change significantly from the measured static weight distribution during riding. The weight distribution for each rider is summarized in Table 2.

Table 2. Weight distribution for each subject.

Parameter	Subject 1	Subject 2
F_{zf}	267 N	311 N
F_{zr}	508 N	556 N

We evaluated the fit of the experimental data to the model predictions statistically by calculating the correlation coefficient between the experimental and theoretical results and to calculate the linear least squares fit of the experimental to theoretical results. We used an alpha level of 0.05 to determine statistical significance.

3 RESULTS

Roll angle. The measured bicycle roll angle is plotted versus normalized lateral acceleration in Figure 10; the roll angle predicted by the model (Equation (7)) for a non-leaning rider ($\varphi_y = 0$) is also plotted for comparison. The non-leaning rider model predicts 99.9% ($\alpha = 0.05$) of the variation of the measured bicycle roll angle for the normal trials without exaggerated rider lean. Moreover, the same model predicts 97.0% ($\alpha = 0.05$) of the variation of the measured bicycle roll angle, regardless of rider posture (normal riding, leaning body into turn, or leaning body out of turn). The linear fit of measured versus predicted bicycle roll angle has a slope that is significantly close to 1.0 (Table 4), which further confirms that this model closely predicts the measured data.

The modest deviations from the model for a non-leaning rider derive from the additional roll of the bicycle caused by a lateral offset of the center of mass of the bicycle-rider system. For example, a rider leaning into a clockwise turn will cause the bicycle roll angle to decrease, resulting in a bicycle roll angle slightly less than that predicted by the non-leaning rider model. Both subjects clearly exhibit this trend, as shown by the dark gray '+' symbols in Figure 10. The opposite trend arises for a rider leaning out of a clockwise turn, as shown by the light gray '×' symbols in Figure 10. If we assume that the measured bicycle roll angle is correct, we can calculate the additional roll of the bicycle caused by a lateral shift in the center of mass (φ_y) using Equation (7). The mean values for the calculated φ_y are reported in Table 3. Both riders were able to create significant additional roll of the bicycle by leaning; on average, the additional roll angle of the bicycle was -2.4 degrees and 2.0 degrees when the riders leaned into and out of the turn, respectively. During normal riding, riders tended to lean slightly into the turn, generating an additional roll angle of merely -0.3 degrees.

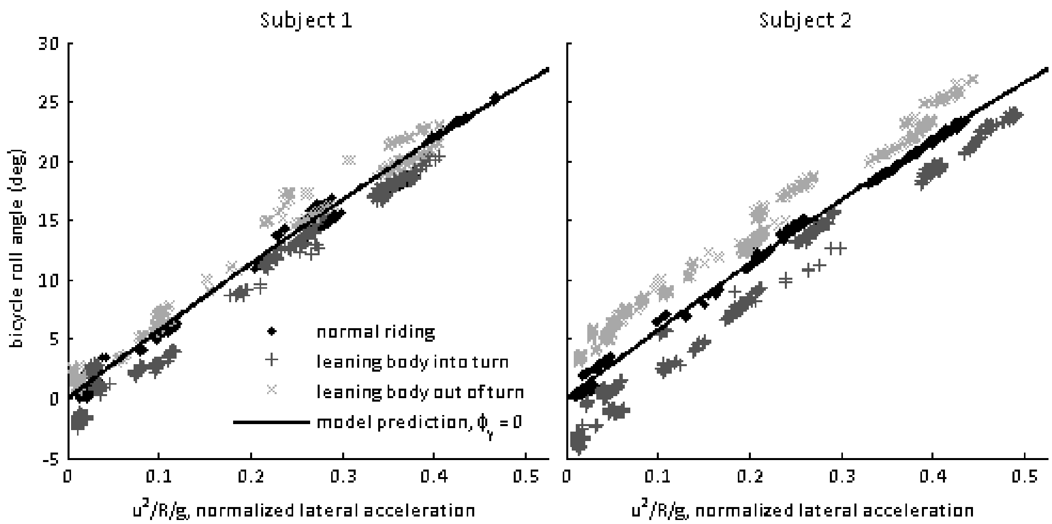

Figure 10. Bicycle roll angle versus normalized lateral acceleration. The experimental data are predicted well by a non-leaning rider model ($R^2 = 0.970, \alpha = 0.05$). Deviation from the model prediction can be interpreted as additional roll of the bicycle caused by a lateral shift in the bicycle-rider system center of mass.

Table 3. Mean calculated values of φ_y from experimental data for different lean conditions

Subject	φ_y, normal riding	φ_y, leaning body into turn	φ_y, leaning body out of turn
1	-0.5°	-1.6°	0.8°
2	0.0°	-2.9°	2.7°
1 & 2	-0.3°	-2.4°	2.0°

Steering angle. The steering angle (δ) is predicted well by the model, as shown in Figure 11. The model, regardless of the tire stiffness values used, provides a good fit to experimental data, as evidenced by the linear fit and R^2 values reported in Table 4. Using tire stiffness values for an idealized tire, the model can explain 99.6% ($\alpha = 0.05$) of the variation in the measured steering angle. Using more realistic tire stiffness values (from Roland [11] and Sharp [19]) did not result in significantly more explained variation, but yields small differences in the linear fits to the data reported in Table 4. Different tire stiffness values do result in different calculated slip angles, ranging from zero degrees for the idealized tire stiffness values to approximately 2.6 degrees for the Roland tire stiffness values. However, as shown in Equation (13), if the slip angles of the front and rear tires are similar, they produce little change in the resulting steering angle. The maximum difference between the calculated slip angles of the front and rear tires was 0.4 degrees, and occurred when using the Roland tire stiffness values. Measured steady turning steering angles ranged in magnitude from approximately zero to 7.5 degrees.

Table 4. Summary of the linear fit ($y = mx + b$) of measured values to model predicted values

Predictor, from model (x)	Predicted variable (y)	Slope (m)	y-intercept (b)	R^2
bicycle roll angle	measured bicycle roll angle	1.00	0.6°	0.970
steering angle, idealized tire	measured steering angle	1.01	-0.2°	0.991
steering angle, Roland tire	measured steering angle	1.04	-0.2°	0.990
steering angle, Sharp tire	measured steering angle	1.03	-0.2°	0.991
steering torque, idealized tire	measured steering torque	1.29	0.12 Nm	0.888
steering torque, Roland tire	measured steering torque	1.31	0.13 Nm	0.896
steering torque, Sharp tire	measured steering torque	1.30	0.12 Nm	0.893

Note: All reported constants from linear fits (m and b) are significantly different than zero and all values of R^2 are significant ($\alpha = 0.05$).

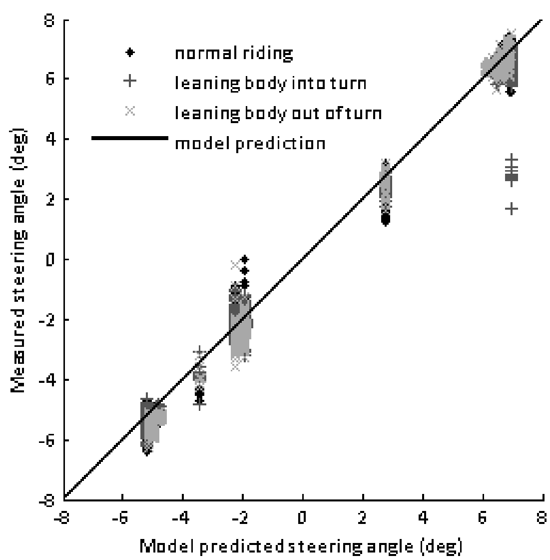

Figure 11. Measured steering angle versus model predicted (using idealized tire stiffness values) steering angle. The experimental data are predicted well by the model when the idealized tire stiffness values are used ($R^2 = 0.991, \alpha = 0.05$). Using more realistic tire stiffness values yields no significant improvement of the model predictions. The clusters of data correspond to the different radii of turns tested experimentally. Scanning from left to right, the data groups correspond to: counter clockwise turning around radii of 12.2, 18.3, 27.4 and 30.5 meters and clockwise turning around turns of 22.9 and 9.1 meters.

Steering torque. The model, using idealized tire parameters, can explain 88.8% ($\alpha = 0.05$) of the variation in the measured steering torque. When the tire stiffness values from Roland are used, the fit to the experimental data is only slightly different, but the difference is significant ($\alpha = 0.05$) and the model can explain 89.6% ($\alpha = 0.05$) of the variation in the measured steering torque. However, the Roland tire stiffness values do not produce results significantly different from the Sharp tire stiffness values. The model, regardless of tire stiffness values used, under-predicts the overall experimental data by approximately 30% (Table 4). However, as shown in Table 5, the accuracy of the predicted value can vary depending on the rider-lean condition; this trend can also be seen in Figure 12. For normal riding, the measured steering torque is over-predicted by approximately 22%, whereas for the rider leaning into the turn the measured steering torque is under-predicted by about 90% (Table 5). Measured steady turning steering torque ranged in magnitude from approximately zero to 2.4 Nm; the average standard deviation for each five-second window of data was 0.74 Nm. Maximum steering torque was measured when the rider leaned out of the turn.

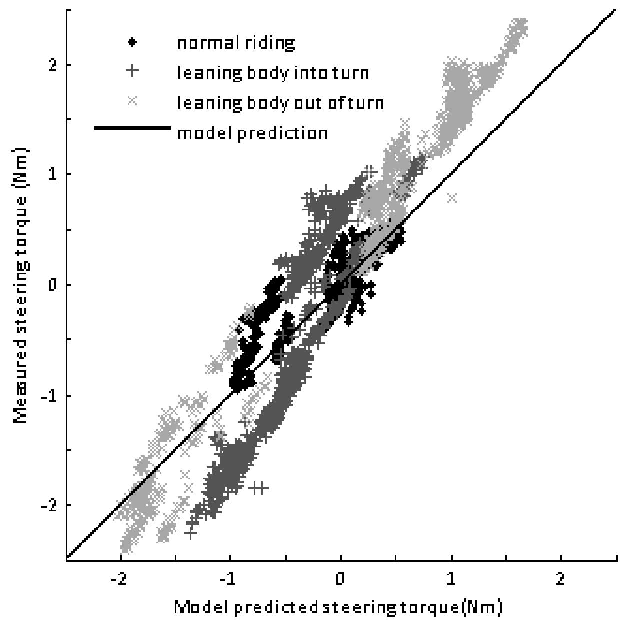

Figure 12. Measured steering torque versus the model predicted (using idealized tire stiffness values) steering torque. The variation of the measured steer torque is predicted well by the model when the idealized tire stiffness values are used ($R^2 = 0.888, \alpha = 0.05$). Using more realistic tire parameters yields no major changes in the predicted variance or the linear fit of the measured values to the model. However, the linear fit of the measured values to the model does change appreciably if each rider-lean condition is examined separately.

Table 5. Summary of the linear fit ($y = mx + b$) of measured steering torque (y) to the predicted steering torque (x) for different rider-lean conditions. The idealized tire stiffness values are used for the model predictions.

Lean condition	Slope (m)	y-intercept (b)	R^2
Normal riding	0.78	0.04 Nm	0.815
Rider lean into turn	1.90	0.26 Nm	0.836
Rider lean out of turn	1.23	0.28 Nm	0.973

Note: All reported constants from linear fits (m and b) are significantly different than zero and all values of R^2 are significant ($\alpha = 0.05$).

Ratio of steering torque and lateral acceleration. The ratio of steering torque and lateral acceleration is plotted versus bicycle speed in Figure 13 for both subjects. The experimental data is plotted for normal riding conditions (black '•'), rider leaning body into the turn (dark gray '+'), and rider leaning body out of the turn (light gray '×'). Example results from the model (curves) are plotted for comparison. As the model is largely insensitive to the selected tire stiffness, we report in Figures 13-14 solutions using the idealized tire. The solution for normal riding is represented by the black solid curve, which is independent of turn radius. The solution for a leaning rider ($\varphi_y \neq 0$) depends on both φ_y and the turn radius. Example solutions are illustrated in Figure 13 for the cases $\varphi_y = \pm 3$ degrees and for a turn radius of 12 meters. In general, these curves shift upward for more negative values of φ_y and larger turn radii; the curves shift downward for more positive values of φ_y and larger turn radii.

The experimental data follows the trends predicted by the model. For a non-leaning rider, the model predicts a negative ratio of steering torque to lateral acceleration, which increases in magnitude at lower speeds. When this ratio is negative, a rider must apply a counter-clockwise steering torque when negotiating a clockwise turn. The experimental data generally follows the same trend; however at low speeds, the variation in the data increases. At lower speeds the lateral acceleration is very small and thus this ratio is very sensitive to small fluctuations in the measured acceleration. Therefore, the model is best compared to the experimental results when the lateral acceleration is significant compared to the acceleration of gravity. For the case of a rider leaning into the turn, both the model and experimental data show that this ratio is positive, meaning that a rider must apply a clockwise steering torque to negotiate a clockwise turn. For the opposite case of a rider leaning out of the turn, both the model and experimental data confirm that this ratio is more negative than in the normal riding condition.

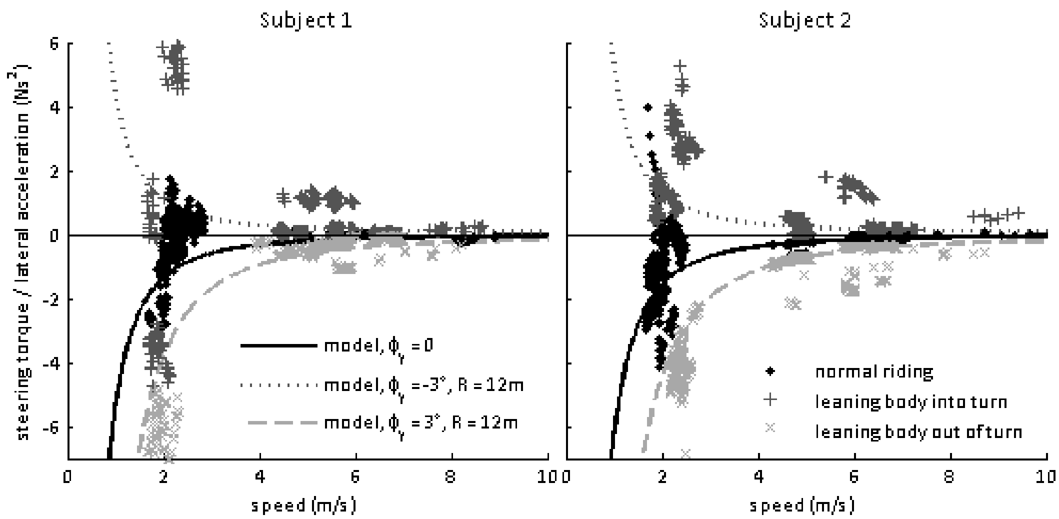

Figure 13. The ratio of steering torque to lateral acceleration versus bicycle speed. Both the model and experimental data show that the ratio of steering torque to lateral acceleration is negative for normal riding (black), more negative for a rider leaning out of the turn (light gray), and positive for a rider leaning into a turn (dark gray). A negative ratio means that a rider must apply a counter-clockwise steering torque to negotiate a clockwise steady turn, whereas a positive ratio means that a rider must apply a clockwise steering torque to negotiate the same turn.

Ratio between steering angle and lateral acceleration. The ratio between the steering angle and lateral acceleration is plotted versus bicycle speed in Figure 14 for both subjects. For comparison, we include a single curve for the model for a non-leaning rider ($\varphi_y = 0$) with idealized tire stiffness values. The model predictions for a leaning rider ($\varphi_y \neq 0$) are virtually indistinguishable from that of the non-leaning rider and are therefore omitted.

The experimental data closely match the model prediction. Both the model and experimental data show that this ratio is positive, regardless of condition, and becomes more positive at lower speeds. A positive ratio means that a rider must maintain a clockwise steering angle when negotiating a clockwise steady-turn; and, for a given lateral acceleration, greater steering angles are required at lower speeds. The experimental data confirm that this ratio is insensitive to rider lean.

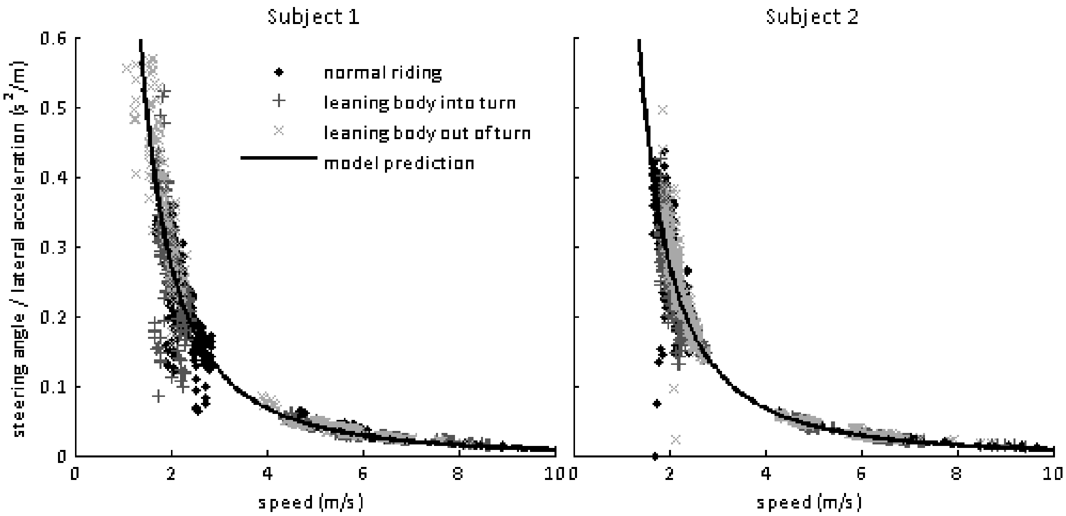

Figure 14. The ratio of steering angle and lateral acceleration versus bicycle speed. The ratio is always positive for both the experimental data and model, indicating that a rider must always steer into a steady-turn. The ratio is insensitive to rider lean.

4 DISCUSSION

As illustrated in Figure 10, the roll angle of the bicycle is predicted well by the simple steady-state turning model developed in Section 2.4. For a motorcycle in steady turning, Fu [5] showed that the roll angle is predicted best when the model includes the gyroscopic effects of the motorcycle wheels and engine, as well as tires with a circular cross-section. In contrast, we found that for a bicycle the roll angle is predicted rather well upon neglecting gyroscopic effects and considering the wheel as a thin disk with a zero-radius edge.

We also demonstrate that a seated rider can generate significant additional roll of a bicycle (Table 3) simply by leaning his/her upper body into or out of a turn. In fact, lean dynamics arise even while riding in a straight line as observed by riders maintaining position on a treadmill [10]. In practice, cyclists often lean their bodies into a turn to increase pedal clearance, such as a road cyclist racing in a criterium. As illustrated in Figure 10, by leaning into the turn, the cyclist decreases the roll angle of the bicycle, and therefore gains pedal clearance. Alternatively, cyclists may lean their bodies out of a turn, as in the case a mountain biker leaning to avoid trees or branches lining the trail. As illustrated in Figure 10, by leaning out of the turn, the cyclist increases the roll of the bicycle but decreases the lateral distance of her/his body from the base of support of the bicycle. The steady-state model is also useful for predicting the changes in steering torque (and the ratio of steering torque to lateral acceleration) when a rider leans into or out of a turn.

The steer angle of the bicycle is predicted well by the model, regardless of the tire stiffness values used; refer to Table 4 and Figure 11. The linear fit of the data to the model results yields values of the slope only slightly greater than one (Table 4), indicating that the model slightly under-predicts the steer angle, regardless of the tire stiffness values. In contrast to these results, Fu [5] observed that for a motorcycle in a steady-turn, the steering angle is over-estimated by a steady state turning model. The y-intercept of the linear fit is approximately -0.2 degrees, regardless of rider lean or tire stiffness values, indicating that perhaps the method of zeroing the steering angle introduced a slight systematic error. The predicted slip angles of the tires ranged from zero (for the idealized tire) to approximately 2.4 degrees (when using tire stiffness values from Roland [11]). However, because the front and rear tires generate near-equal slip, there is little net effect on the steering angle of the bicycle. Therefore, the presence of side-slip while riding a bicycle is not likely to be detected by a rider through the steering angle.

The steady-state turning model reasonably predicts the steering torque of a bicycle. The model explains 88.8% of the variation in the measured data and correctly predicts the reversal of the steering torque. However, the model tends to under-predict the measured steer torques by approximately 30%. This discrepancy might be reduced by adopting more detailed, multi-body models of Cossalter et al. [20] and Sharp [19], among others [6, 7, 17, 21, 22]. However, the discrepancy might also arise from the measurement limitations of the current torque sensor. In particular, all measured steering torques were less than 10% of the full scale range of the sensor, rendering the torque measurements sensitive to both small systematic and random error sources. The steering torque required to steer a bicycle around a steady curve is substantially smaller than that for a motorcycle; we measured a maximum steering torque of 2.4 Nm for the tested conditions, whereas Bortoluzzi et al. [23] measured steering torques up to 9 Nm for a motorcycle with a non-leaning rider. In addition, the steering torque during each five second window varied significantly, with an average standard deviation of 0.74 Nm. Another source of error could derive from the fact that the steering torque is very sensitive to the camber angle of the front tire. In particular, errors in the measured bicycle roll angle translate to errors in the computed camber angle and thus errors in the calculated steering torque.

The ratio of the steering torque to the lateral acceleration, or acceleration index, has been identified in the motorcycle handling literature as an important measure of maneuverability [6-8]. For a motorcycle, the ratio defines the gain between the dominant control input (steer torque) and the vehicle response (lateral acceleration). Similar to the motorcycle steady turning results of Bortoluzzi et al. [7], we found that the steering torque/lateral acceleration ratio follows the trends predicted by a steady turning model. Both our experimental and theoretical results also confirm the theoretical findings of Bortoluzzi et al., which demonstrate that the lateral displacement of a rider's center of mass has a significant effect on the steering torque/lateral acceleration ratio.

Our experimental and theoretical results demonstrate that a rider can significantly change the steering torque required to negotiate a steady-turn by simply leaning into or out of the turn. Leaning into the turn can produce a dramatic effect, namely the complete reversal of the required steering torque. The steering torque governed by Equation (17) is primarily a function of: 1) the vertical force on the front tire, 2) the lateral force on the front tire, and 3) the camber angle of the front tire. For a non-leaning rider, the vertical force remains the dominant contributor to the steering torque and this contribution yields a negative steering torque. However, if the roll of the bicycle (and therefore the camber angle of the front tire) is changed by a leaning rider, the lateral force can become the dominant contributor and reverse the sign of the steering torque. Several models have been derived to explore how a rider is able to ride a bicycle with no-hands, i.e., ride with zero steering torque [9, 19, 24]. These models incorporate the lean (reaction) torque that is applied between the rider's upper body and the bicycle. While we have not measured this lean torque, we clearly demonstrate that upper body lean can be used to control the sign as well as the magnitude of the steering torque required to negotiate a steady-turn. Therefore, it is also possible for a rider to adjust his/her body lean to achieve zero steering torque, thereby enabling no-handed riding. Similarly, for "hands-on" riding, a rider may adjust his/her lean to control the steering torque.

The above discussion suggests that the steering torque is not an easy quantity for a rider to predict. For instance, a rider can simply change the required control strategy from applying a steer torque out of the turn to applying a steer torque into a turn by leaning out of a turn. In addition, a dynamically leaning rider constantly changes the steering torque/lateral acceleration ratio by simple pedaling and shifting weight from side-to-side. A more predicable relation between a control action and bicycle response is suggested by the steering angle/lateral acceleration ratio. This ratio is always positive and follows the same curve, regardless of rider lean. This suggests that steering angle is a better control action than steering torque.

The steady-state turning model represents a useful tool for evaluating the maneuverability and handling characteristics of bicycles. The model can be further used to explore how changes in bicycle parameters (wheelbase, steer axis tilt, wheel size, fork rake, trail, and weight distribution) affect the steering angle and the steering torque required of the rider during steady turning as well as how rider lean can be used to control the bicycle. A major benefit of this simple model is that it does not require knowledge of the inertial properties of the wheels, rider, or bicycle frame—only the weight distribution needs to be known. Simple models of bicycle control have been used to design bicycles that are intentionally unrideable [25] as well as bicycles that make it easier for new riders to learn how to ride a bike [25, 26]. Similarly, the model developed here could be useful for optimizing the maneuverability and handling characteristics of bicycles, perhaps for specific populations. Along with simple models that predict bicycle stability [1] and controllability [25], the model here forms part of larger toolbox that may enable scientists and bicycle designers to quantify bicycle performance characteristics and the control preferences of the human rider.

5 SUMMARY AND CONCLUSION

We investigated the steady-state handling of a bicycle as the means to explore the major factors governing the maneuverability and handling characteristics of a rider/bicycle system. Steady-state handling arises when the rider/bicycle negotiates a constant radius turn at constant speed and lean. We employed a bicycle instrumented to measure steering torque, steering angle, bicycle speed, bicycle acceleration, and bicycle angular velocity. We collected data for two subjects during steady-turning around six different radii turns (9.14, 12.19, 18.29, 22.86, 27.43, and 30.48 meters), three speed conditions (slow, medium, and fast), and three rider lean conditions (normal rider lean, exaggerated lean into the turn, and exaggerated lean out of the turn). We then introduced a model for the steady-state handling of the bicycle/rider system, which allows for rider lean, and compared the experimental data to the model predictions. Specifically, we compared: bicycle roll angle, steering angle, steering torque, steering torque/lateral acceleration ratio, and steering angle/lateral acceleration ratio.

The model is a useful tool for understanding the maneuverability and handling characteristics of a pedaled bicycle in a real-world environment. The model, with idealized tire parameters, explains 97.0% of the variability in the measured bicycle roll angle, 99.6% of the variability in the measured steering angle, and 88.8% of the variability in the measured steering torque. Using more realistic tire parameters yields little difference in the model predictions. Both the model and data demonstrate that rider lean (lateral shifting of the bicycle/rider center of mass) strongly influences the steering torque/lateral acceleration ratio, suggesting that rider lean plays an important role in the control of a bicycle. By contrast, the steering angle/lateral acceleration ratio is largely insensitive to rider lean, suggesting that using the steering angle as a cue for bicycle control is advantageous over using steering torque.

ACKNOWLEDGEMENTS

We thank Dexter Bike and Sport for donated and discounted bicycle parts required for the instrumented bicycle and thank Kevin King and Ryan McGinnis for their assistance in calibrating the inertial measurement unit.

REFERENCES

[1] J. P. Meijaard, *et al.*, "Linearized dynamics equations for the balance and steer of a bicycle: a benchmark and review," *Proceedings of the Royal Society A: Mathematical, Physical and Engineering Science,* vol. 463, pp. 1955-1982, August 8, 2007.

[2] J. Moore and M. Hubbard, "Parametric Study of Bicycle Stability (P207)," in *The Engineering of Sport 7*, ed: Springer Paris, 2008, pp. 311-318.

[3] P. Basu-Mandal, *et al.*, "Hands-free circular motions of a benchmark bicycle," *Proceedings of the Royal Society A,* vol. 463, pp. 1983-2003, 2007.

[4] D. L. Peterson and M. Hubbard, "General steady turning of a benchmark bicycle model," in *the ASME 2009 International Design Engineering Technical Conferences and 7th International Conference on Multibody Systems, Nonlinear Dynamics, and Control*, San Diego, USA, 2009.

[5] H. Fu, "Fundamental Characteristics of Single-Track Vehicles in Steady Turning," *Bulletin of the Japan Society of Mechanical Engineers,* vol. 9, pp. 284-293, 1966.

[6] V. Cossalter, *et al.*, "Steady turning of two-wheeled vehicles," *Vehicle System Dynamics,* vol. 31, pp. 157-182, 1999.

[7] D. Bortoluzzi, *et al.*, "Experimental investigation and simulation of motorcycle turning performance," in *3rd International Motorrad-konferenzen*, Monaco, 2000.

[8] J. W. Zellner and D. H. Weir, "Development of handling test procedures for Motorcycles," SAE, 1978.

[9] D. L. Peterson and M. Hubbard, "Yaw Rate and Velocity Tracking Control of a Hands-Free Bicycle," *ASME Conference Proceedings,* vol. 2008, pp. 447-454, 2008.

[10] J. K. Moore, *et al.*, "Rider motion identification during normal bicycling by means of principal component analysis," in *MULTIBODY DYNAMICS 2009, ECCOMAS Thematic Conference*, Warsaw, Poland, 2009.

[11] R. D. Roland, "Computer simulation of bicycle dynamics," in *Mechanics and Sport*, J. L. Bleustein, Ed., ed: ASME, 1973, pp. 35-83.

[12] A. W. Jackson and M. Dragovan, "An experimental investigation of bicycle dynamics," unpublished, 1998.

[13] K. Y. Cheng, *et al.*, "Bicycle torque sensor experiment," University of California, Santa Barbara, 2003.

[14] J. D. G. Kooijman, *et al.*, "Experimental validation of a model of an uncontrolled bicycle," *Multibody System Dynamics,* vol. 19, pp. 115-132, 2008.

[15] J. D. G. Kooijman and A. L. Schwab, "Some Observations on Human Control of a Bicycle," in *11th mini Conference on Vehicle System Dynamics, Identification and Anomalies*, Budapest, Hungary, 2008.

[16] K. W. King, "The design and application of wireless MEMS inertial measurement units for the measurement and analysis of golf swings," Ph. D., Mechanical Engineering, University of Michigan, Ann Arbor, MI, 2008.

[17] H. B. Pacejka, *Tyre and vehicle dynamics*. Oxford: Butterworth-Heinemann, 2002.

[18] J. Y. Wong, *Theory of ground vehicles*, 2nd ed. New York, N.Y.: J. Wiley, 1993.

[19] R. S. Sharp, "On the Stability and Control of the Bicycle," *Applied Mechanics Reviews,* vol. 61, p. 060803, 2008.

[20] V. Cossalter*, et al.*, "Motorcycle steering torque decomposition," in *World Congress on Engineering*, London, UK, 2010.

[21] D. J. N. Limebeer and R. S. Sharp, "Bicycles, motorcycles, and models," *IEEE Control Systems Magazine,* vol. 26, pp. 34-61, 2006.

[22] R. S. Sharp*, et al.*, "Advances in the Modelling of Motorcycle Dynamics," *Multibody System Dynamics,* vol. 12, pp. 251-283, 2004.

[23] D. Bortoluzzi*, et al.*, "Motorcycle steady turning: the significance of geometry and inertia," in *FISITA 7th International Conference - The Role of Experimentation in the Automotive Product Development Process*, Firenze, Italy, 2001.

[24] A. L. Schwab*, et al.*, "Some recent developments in bicycle dynamics and control," in *Fourth European Conference on Structural Control (4ECSC), Institute of Problems in Mechanical Engineering, Russian Academy of Sciences*, St. Petersburg, Russia, 2008, pp. 695–702.

[25] K. J. Astrom*, et al.*, "Bicycle dynamics and control: adapted bicycles for education and research," *IEEE Control Systems Magazine,* vol. 25, pp. 26-47, 2005.

[26] R. E. Klein*, et al.*, "Adapted bicycles for teaching riding skills," *Teaching Exceptional Childern,* vol. 37, pp. 50-56, 2005.